IEIE Transactions on Smart Processing and Computing, vol. 4, no. 5, October 2015
http://dx.doi.org/10.5573/IEIESPC.2015.4.5.305

Design and Simulation of Depth-Encoding PET Detector using Wavelength-Shifting (WLS) Fiber Readout

Su Jung An, Hyun-il Kim, Chae Young Lee, Han Kyeol Song, Chan Woo Park, and Young Hyun Chung*

Department of Radiological Science, Yonsei University / Wonju, South Korea
crystal8374@yonsei.ac.kr, hyunil@yonsei.ac.kr, lcy225@yonsei.ac.kr, shg2848@yonsei.ac.kr, cksdn9432@yonsei.ac.kr, ychung@yonsei.ac.kr

* Corresponding Author: Young Hyun Chung

Received October 14, 2015; Revised October 21, 2015; Accepted October 25, 2015; Published October 31, 2015

** Regular Paper*

***Abstract*:** We propose a new concept for a depth of interaction (DOI) positron emission tomography (PET) detector based on dual-ended-scintillator (DES) readout for small animal imaging. The detector consists of lutetium yttrium orthosilicate (LYSO) arrays coupled with orthogonal wavelength-shifting (WLS) fibre placed on the top and bottom of the arrays. On every other line, crystals that are 2 mm shorter are arranged to create grooves. WLS fibre is inserted into these grooves. This paper describes the design and performance evaluation of this PET detector using Monte Carlo simulations. To investigate sensitivity by crystal size, five types of PET detectors were simulated. Because the proposed detector is composed of crystals with three different lengths, degradation in sensitivity across the field of view was also explored by simulation. In addition, the effect of DOI resolution on image quality was demonstrated. The simulation results proved that the devised PET detector with excellent DOI resolution is helpful for reducing the channels of sensors/electronics and minimizing gamma ray attenuation and scattering while maintaining good detector performance.

***Keywords*:** Computer-aided design, Modelling, Monte-carlo simulation, Positron emission tomography (PET), Depth of interaction (DOI)

1. Introduction

As the importance of animal model–based research has increased [1], dedicated small-animal positron emission tomography (PET) scanners have been actively developed [2-10]. The small-animal PET scanner has a small ring diameter and contains both thin and long scintillation crystals to enhance sensitivity and spatial resolution [11]. It degrades spatial resolution at the peripheral region of the field of view (FOV) due to parallax error. The parallax error can be reduced by measuring the interaction point of photons along the crystal length [12]. Many depth of interaction (DOI)-encoding methods have been proposed [13-19].

One promising DOI detection method is a dual-ended-scintillator (DES) readout, which employs two photosensors on both ends of a scintillator array and measures the signal ratio from sensors at each end to determine DOI [20, 21]. This approach provides continuous DOI information. According to recent reports, DOI resolution of 2 mm can be achieved with this technique [22, 23]. However, the DES readout technique requires additional photosensors and electronics to acquire DOI information [24]. They demand more resources for signal readout (e.g. Analog-to-digital converter (ADC) and Field programmable gate array (FPGA)). These requirements also increase cost. Even with advances in these devices, there are still problems regarding heat generation and the large number of interconnections required to implement a large number of channels. Gamma ray attenuation and scattering caused by photosensors and electronics at the front of the crystal array should also be considered [25].

We propose a new concept DOI PET detector with a drastically reduced number of readout channels. Our method is based on a DES readout technique using a wavelength shifting (WLS) fiber readout. In this paper, we describe the detector concept and assess performance with Monte Carlo simulations.

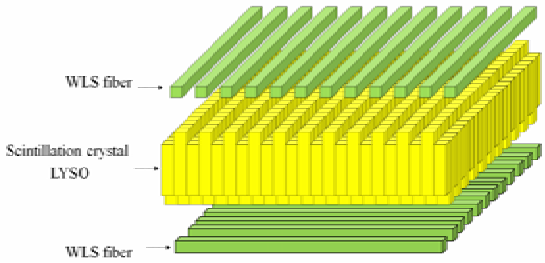

Fig. 1. Schematic of DOI-encoding detector module composed of a 23 × 23 array of LYSO crystal readout by 2 × 2 × 46 mm^3 WLS fibers.

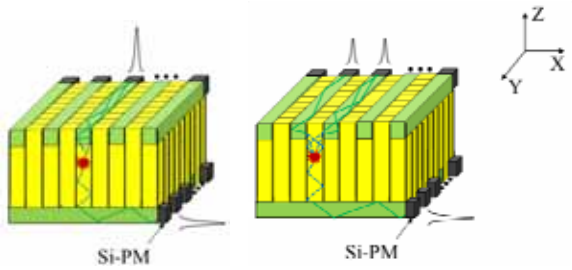

(a) (b)

Fig. 2. The principle of crystal identification in a detector module: (a) Crystal pixels placed in odd rows can be identified by finding the photosensor showing the largest signal, (b) Light photons generated in pixels of even rows can be detected by two adjacent WLS fibers.

2. Materials and methods

2.1 Detector design

The detector is based on a 23 × 23 array of lutetium yttrium orthosilicate (LYSO) crystals coupled with 2 × 2 × 46 mm^3 WLS fibers. The crystal elements have three different sizes: 2 × 2 × 16 mm^3, 2 × 2 × 18 mm^3, and 2 × 2 × 20 mm^3. As shown in Fig. 1, on every other line, crystals that are 2 mm shorter are arranged in the X-direction on top and the Y-direction on the bottom of the array to create grooves for WLS fiber insertion. WLS fibers are inserted into these grooves, and one end of each WLS fiber is coupled to a single-channel photosensor for detection of scintillating lights trapped in the fiber. By photon absorption and re-emission in WLS fibers, light photons entering the WLS fiber are channeled toward the photosensor so that X and Y locations of gamma interac-tion can be determined [26].

Crystal pixels placed in odd rows can be identified by finding the photosensor showing the largest signal, as illustrated in Fig. 2(a). In contrast, light photons generated in pixels of even rows can be detected by two adjacent WLS fibers, as shown in Fig. 2(b). Continuous DOI information is acquired from the ratio of signals at either end of the array.

2.2 Monte Carlo simulation of scanner geometries

The Geant4 Application for Emission Tomography (GATE) Monte Carlo simulator was used to evaluate the performance of the detectors [27]. Fig. 3 shows the simulated detector geometry. The simulated small-animal PET scanner has an inner diameter of 80 mm, an axial FOV of 46 mm, and is composed of six detectors in a ring. The detector design is described in Section 2.1. WLS fibers were set to polystyrene with 1.05 g/cm³ density. Table 1 summarizes the parameters of the simulated PET detectors.

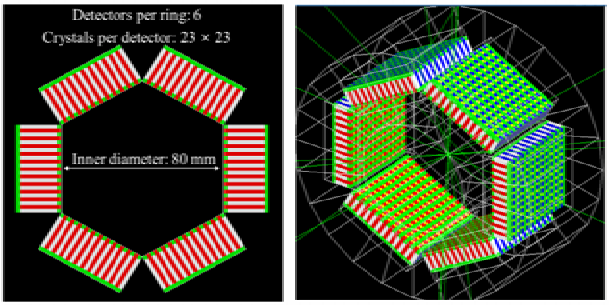

Fig. 3. Schematics for GATE simulation of scanner geometries. The simulated small-animal PET scanner has an inner diameter of 80 mm, an axial FOV of 46 mm, and is composed of six detectors in a ring.

Table 1. Parameters of simulated PET detectors.

Parameter	New DOI PET scanner	
Crystal material	LYSO	
Crystal size	2 × 2 × 16 mm^3	
	2 × 2 × 18 mm^3	
	2 × 2 × 20 mm^3	
Crystal array	23 × 23 (crystals/ module)	2 × 2 × 16 mm^3 × 144
		2 × 2 × 18 mm^3 × 264
		2 × 2 × 20 mm^3 × 121
WLS fiber	2 × 2 × 46 mm^3 Top: 12, Bottom 12 (Total: 24)	
Number of detectors	6 (1 ring)	
Number of crystals	3174	
Ring diameter	80 mm	
Axial FOV	46 mm	

2.3. Sensitivity

Sensitivity was defined as the percentage of total events that were recorded as coincidence events. A 1.11-MBq point source emitting mono-energetic back-to-back 511-keV photons was positioned at the center of the FOV, and acquisition time was set to 5 s. All simulations in this paper were performed with a coincidence window of 10 ns and energy resolution of 26%.

To estimate sensitivity depending on crystal size, five different types of detectors were simulated. The crystal sizes of the simulated detectors are summarized in Table 2. As mentioned in previous sections, on every other line, crystals that are 2 mm shorter are arranged in the X-direction on the top of the array and the Y-direction on the bottom. All detectors have identical scanner radii.

Table 2. Crystal sizes of simulated detectors for sensitivity analysis.

Detector	Crystal array
Detector 1	2 × 2 × 10 mm^3 × 144 2 × 2 × 12 mm^3 × 264 2 × 2 × 14 mm^3 × 121
Detector 2	2 × 2 × 12 mm^3 × 144 2 × 2 × 14 mm^3 × 264 2 × 2 × 16 mm^3 × 121
Detector 3	2 × 2 × 14 mm^3 × 144 2 × 2 × 16 mm^3 × 264 2 × 2 × 18 mm^3 × 121
Detector 4	2 × 2 × 16 mm^3 × 144 2 × 2 × 18 mm^3 × 264 2 × 2 × 20 mm^3 × 121
Detector 5	2 × 2 × 18 mm^3 × 144 2 × 2 × 20 mm^3 × 264 2 × 2 × 22 mm^3 × 121

Sensitivity was measured in three energy windows around the 511-keV photo-peak. The upper level discriminator (ULD) was set to 650 keV, whereas the lower level discriminator (LLD) was set to 250, 350 and 450 keV.

The proposed detector is composed of crystals with three different lengths. This may change the sensitivity pattern across the FOV. Therefore, sensitivity across the FOV was evaluated by varying the radial offset of a point source from -16 mm to +16 mm at 2-mm intervals and by varying the axial offset from -15 mm to +15 mm at 5-mm intervals. The results were compared with three traditional cuboid detectors consisting of 23 × 23 arrays of 2 × 2 × 16 mm^3, 2 × 2 × 18 mm^3, and 2 × 2 × 20 mm^3. The energy window was set to 350-650 keV.

2.4 Spatial resolution according to DOI resolution

A 5.55-MBq point source emitting mono-energetic back-to-back 511-keV photons was simulated. The source location was varied from the FOV center to a 32-mm offset at 4-mm intervals in the radial direction. From GATE simulations, the location of the center of mass for the interaction of annihilation photons in the scintillator was acquired [28]. In the case of a gamma multiple hits Pi, i = 1, …, n, each with energy mi that are located in a space with coordinates ri, i = 1, …, n, the coordinates R of the position are calculated as

$$R = \frac{1}{M}\sum_{i=1}^{n} miri \qquad \text{(Eq. 1)}$$

where M is the sum of the energies of all of the gamma reactions.

To model a finite DOI resolution, the data were sorted into 20, 10, 4, 2 and 1 (no DOI) DOI bins (corresponding to 1, 2, 5, 10 and 20 mm DOI resolution, respectively). Fig. 4 shows sorted DOI bins to demonstrate the effects of DOI resolution on image quality.

Sinograms were generated using sorted coincidence events corresponding to the DOI bin. The images were reconstructed using two-dimensional filtered back-projection (FBP) with a ramp filter, and full-width at half-maximum (FWHM) was measured for radial and transverse (tangential) directions.

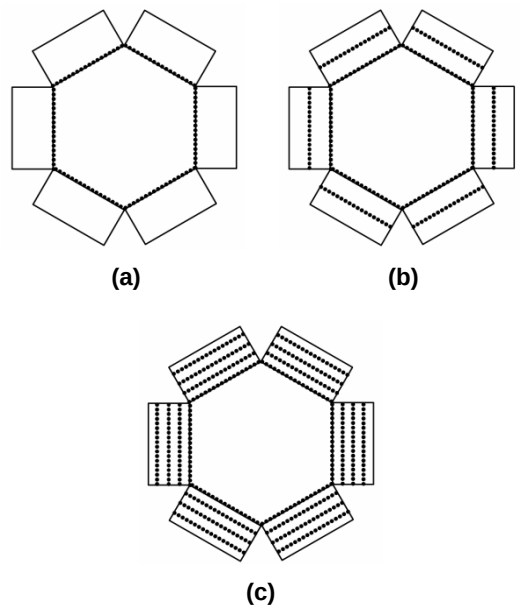

Fig. 4. The sorted DOI bins for demonstrating the effects of DOI resolution on image quality. (a) 1 DOI bin (no DOI), (b) 2 DOI bins (10 mm DOI resolution), (c) 4 DOI bins (5 mm DOI resolution)

Table 3. Sensitivity depending on crystal length for three energy windows.

Crystal length (mm)	250-650 keV	350-650 keV	450-650 keV
10-12-14	3.24%	2.90%	1.52%
12-14-16	4.09%	2.97%	2.00%
14-16-18	4.93%	3.64%	2.49%
16-18-20	5.73%	4.31%	2.96%
18-20-22	6.51%	4.99%	3.44%

3. Results

3.1. Sensitivity

Simulated sensitivity values with different crystal lengths are summarized in Table 3. Crystals with three different lengths were used for WLS fiber insertion. The reported sensitivity was 4%, 2%-4% and 3.8% for the GE eXplore Vista PET system [29], Gamma Medica-Ideas PET system [30] and ClearPET LYSO/LuYAP phoswich scanner [31], respectively, at the center of the FOV with a lower level discriminator setting of 250 keV. The sensitivity of the proposed scanner with a 16-18-20 mm crystal length is comparable to that of commercial state-of-the-art systems with a 350-650 keV energy window.

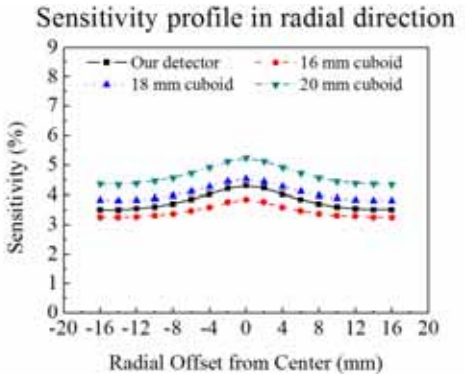

(a)

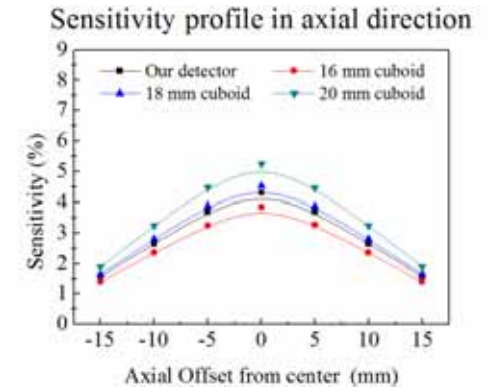

(b)

Fig. 5. Sensitivity was measured with 1.11-MBq mono-energetic back-to-back 511-keV photons (a) at 4-mm increments in the radial direction and (b) at 5-mm increments in the axial direction.

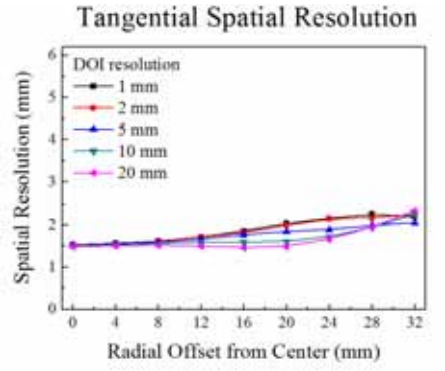

(a)

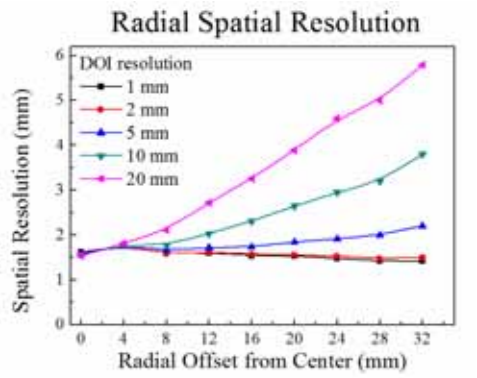

(b)

Fig. 6. (a) Tangential and (b) radial spatial resolution for varying DOI resolutions across the FOV.

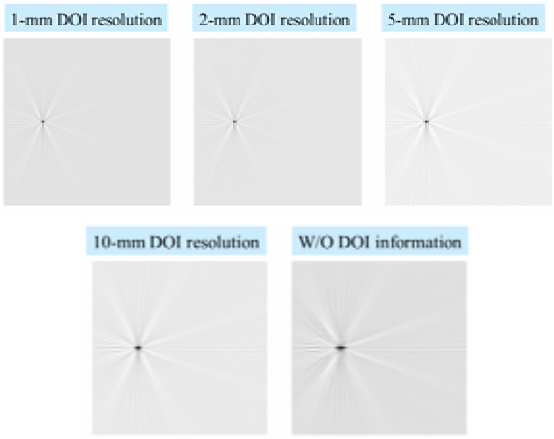

Fig. 7. Reconstructed images of point sources located at a radial offset of 32 mm from the center of the FOV employing different DOI resolutions.

Figs 5(a) and (b) , respectively, illustrate sensitivity measured with 1.11-MBq mono-energetic back-to-back 511-keV photons at 4-mm increments in the radial direction and 5-mm increments in the axial direction. This shows that maximum sensitivity is found at the center of the FOV. The sensitivity pattern of the proposed scanner was similar to that of a traditional cuboid scanner across the entire FOV. The comparison shows that the sensitivity of the proposed scanner is greater than the sensitivity of the scanner based on cuboid arrays with a 16-mm crystal length, less than that of a 20-mm crystal length cuboid scanner, and close to that of a cuboid scanner with an 18-mm crystal length.

3.2. Spatial resolution according to DOI resolution

Spatial resolution with varying DOI resolutions across the FOV is shown in Fig. 6. The tangential spatial resolution was not considerably degraded by source position and DOI resolution, and it remained 2 mm FWHM. However, radial spatial resolution depends strongly on source radial position and DOI resolution.

Figs 7 and 8, respectively, describe reconstructed images and profiles of point sources located at a radial offset of 32 mm from the center of the FOV employing different DOI resolutions.

4. Discussion and conclusion

Simulation results indicate that the proposed system has sensitivity in the same range as state-of-the-art small-animal PET systems, and the pattern of sensitivity did not degrade significantly across the FOV. As expected, improved DOI resolution led to considerably improved uniformity in radial resolution. A small-animal PET scanner with a diameter of 80 mm and 16-, 18-, and 20-

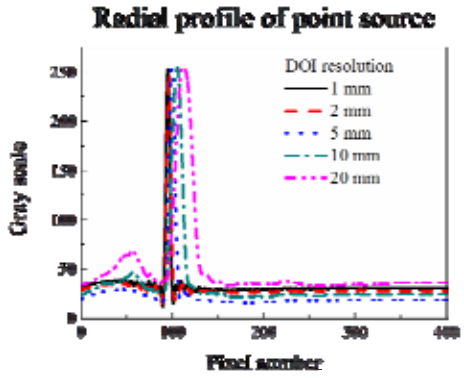

Fig. 8. Radial profile of point sources located at a radial offset of 32 mm from the center of the FOV.

mm-long crystals shows uniform spatial resolution across the FOV when the DOI resolution of the detector is better than 5 mm.

In this work, light transportation through the WLS fiber did not affect light collection efficiency and wavelength shifting efficiency. Loss of light collection with the use of WLS fibers is a significant problem that may degrade both spatial and energy resolution. In the next study, we will investigate the effect of light collection with WLS fibers on detector performance.

We propose a new DOI encoding detector design that allows N^2 crystals to be decoded with just (N+1)/2N channels of sensors and electronics. Using this method, the channels of sensors and electronics can be reduced dramatically. Furthermore, the described detector design separates photosensors from detectors using a WLS fiber readout. This minimizes gamma ray attenuation and scattering caused by photosensors and electronics. We expect this design to solve the problems surrounding DES readout while maintaining competitive detection performance.

Acknowledgement

This work was supported by the BK21 Plus program through the National Research Foundation (NRF) funded by the Ministry of Education of Korea (22A20130012172).

References

[1] R. Yao et al., "Small-animal PET: what is it, and why do we need it?," *J. Nucl. Med. Techno*, Vol. 40, pp. 157–165, May 2012. Article (CrossRefLink)

[2] P. D. Cutler et al., "Design features and performance of a PET system for animal research," *Journal of Nuclear Medicine* Vol. 33, pp. 595-604, April 1992. Article (CrossRefLink)

[3] M. Watanabe et al., "A high resolution PET for animal studies" *IEEE Trans. Med. Imag*. Vol. 11, no. 4, pp. 577-580, December 1992. Article (CrossRefLink)

[4] S. R. Cherry et al., "MicroPET: a high resolution PET scanner for imaging small animals," *IEEE Trans. Nucl. Sci*. Vol. 44, no. 3, pp. 1161-1166, Jun 1997. Article (CrossRefLink)

[5] M. Bergeron et al., "Performance evaluation of the LabPET APD-based digital PET scanner," *IEEE Trans. Nucl. Sci*. Vol. 56, no. 1, pp 10-16, February 2009. Article (CrossRefLink)

[6] H. W. de Jong et al., "Performance evaluation of the ECAT HRRT: an LSO-LYSO double layer high resolution, high sensitivity scanner," *Phys. Med. Biol*. Vol. 52, no. 4, pp. 1505-1526, February 2007. Article (CrossRefLink)

[7] Y. Wang et al., "Performance evaluation of the GE Healthcare eXplore VISTA dual-ring small-animal PET scanner," *J. Nucl. Med*. Vol. 47, no. 11, pp. 1891-1900, November 2006. Article (CrossRef Link)

[8] J. Seidel et al., "Resolution uniformity and sensitivity of the NIH ATLAS small animal PET scanner: comparison to simulated LSO scanners without depth-of-interaction capability," *IEEE Trans. Nucl. Sci*. Vol. 50, no. 5, pp. 1347-1350, October 2003. Article (CrossRef Link)

[9] S. Surti et al., "Design evaluation of A-PET: a high sensitivity animal PET camera," *IEEE Trans.Nucl. Sci*. Vol. 50, no. 5, pp. 1357-1363, October 2003. Article (CrossRef Link)

[10] K. Ziemonsa et al., "The ClearPET™ project: development of a 2nd generation high-performance small animal PET scanner," *Nucl. Instrum. Methods Phys. Res. A* Vol. 537, no. 1-2, pp. 307-311, January 2005. Article (CrossRef Link)

[11] H. Peng et al., "Recent developments in PET," *Instrumentation Curr Pharm Biotechnol*. vol. 11, no. 6, pp. 555-571, July 2010. Article (CrossRef Link)

[12] S.R. Cherry et al., Physics in Nuclear Medicine 3rd ed. (Saunders) pp. 334-336, 2003

[13] J. Zhang et al., "Study of the performance of a novel 1 mm resolution dual-panel PET camera design dedicated to breast cancer imaging using Monte Carlo simulation," *Med. Phys*. Vol. 34, no. 2, pp. 689-702, 2007. Article (CrossRef Link)

[14] T. Tsuda et al., "A four-layer depth of interaction detector block for small animal PET," *IEEE Trans. Nucl. Sci*. Vol. 51, no. 5, pp. 2537-2542, October 2004. Article (CrossRef Link)

[15] Y.H. Chung et al., "Performance measurements of a depth-encoding TraPET detector module," *Jinst.* Vol. 6 C11032, November 2011. Article (CrossRef Link)

[16] M. Ito et al., "Continuous depth-of-interaction measurement in a single-layer pixelated crystal array using a single-ended readout." *Phys. Med. Biol*. Vol. 58, no. 5, pp. 1269-1282, 2013. Article (CrossRef Link)

[17] Y. H. Chung et al., "Preliminary experimental results of a quasi-monolithic detector with DOI capability for a small animal PET," *Nucl. Instrum. Methods Phys. Res. A*, Vol. 621, no. 1-3, pp. 590-594, September 2010. Article (CrossRef Link)

[18] Y.H. Chung et al., "TraPET: High performance small animal PET with trapezoidal phoswich detector," *Nucl. Instrum. Methods Phys. Res. A* Vol. 652, pp. 802-805, October 2011. Article (CrossRef Link)

[19] M Ito et al., "Positron Emission Tomography (PET)

Detectors with Depth-of-Interaction (DOI) Capability," *Biomed Eng Lett*. Vol. 1, no. 2, pp. 70-81, May 2011. Article (CrossRef Link)
[20] Y. Shao et al., "A novel method to calibrate DOI function of a PET detector with a dual-ended-scintillator readout," *Med. Phys*. Vol. 35, no. 12, pp. 5829-5840, 2008. Article (CrossRef Link)
[21] A. Kishimoto et al., "Development of a dual-sided readout DOI-PET module using large-area monolithic MPPC-arrays," *IEEE Trans Nucl Sci*. Vol. 60, pp. 38-43, 2013. Article (CrossRef Link)
[22] M.C. Abreu et al., "Design and evaluation of the clear-PEM scanner for positron emission mammography," *IEEE Trans. Nucl. Sci*. Vol. 53, no. 1, pp. 71-77, February 2006. Article (CrossRef Link)
[23] Y. Yang et al., "A prototype PET scanner with DOI-encoding detectors," *J. Nucl. Med* vol. 49, pp. 1132-1140, July 2008. Article (CrossRef Link)
[24] M. Ito et al., "Design and simulation of a novel method for determining depth-of-interaction in a PET scintillation crystal array using a single-ended rea-dout by a multi-anode PMT," *Phys. Med. Biol*. Vol. 55, no. 13, pp. 3827-3841, 2010. Article (CrossRef Link)
[25] T.K. Lewellen et al., "Recent developments in PET detector technology," *Phys. Med. Biol*. Vol. 53, no. 17, pp. R287-317, August 2008. Article (CrossRef Link)
[26] H. Du et al., "Comparison of four depth-encoding PET detector modules with wavelength shifting (WLS) and optical fiber read-out," *Phys. Med. Biol*. Vol. 53, no. 7, pp. 1829-1842, March 2008. Article (CrossRef Link)
[27] S. Jan et al., "GATE: a simulation toolkit for PET and SPECT," *Phys. Med. Biol*. Vol. 49, pp. 4543-4561, September 2004. Article (CrossRef Link)
[28] GATE User Guide. Available at Article (CrossRef Link)
[29] GE-Suinsa. Madrid (Spain). Available at: Article (CrossRef Link)
[30] Gamma Medica-Ideas. Northridge, CA. Availableat: Article (CrossRef Link)
[31] Raytest GmbH. Straubenhardt (Germany).Available at: Article (CrossRef Link)

Su Jung An is a Ph.D. student in the Molecular Imaging Lab in the Department of Radiological Science, Yonsei University, Republic of Korea. She received her BSc in radiological science from Yonsei University, Korea, in 2009. She has been working on development of a positron emission tomography imaging system. As a Ph.D. student, she has been involved in all parts of this research, from detector and data acquisition system design to detector performance measurement, and optimizing acquisition parameters for PET imaging.

Hyun-Il Kim is a post-doctorate researcher at Yonsei University in the Republic of Korea. He received a Ph.D. in radiological science from Yonsei University in 2015. He worked at Nucare Medical Systems, Inc. and at the Korea Institute of Radiological and Medical Sciences (KIRAMS) as a researcher. His current research interests include positron emission tomography (PET) systems, small-animal PET, and ion-beam therapy monitoring.

Chae Young Lee received a BSc from the department of radiological science at Yonsei University, South Korea, in 2011. He is currently pursuing his combined master's and doctorate in the molecular imaging laboratory at the same university. His research interests include proton therapy, PET and gamma camera systems.

Han Kyeol Song received a BSc from the department of biomedical engineering at Jungwon University, South Korea, in 2012. He is in the ongoing doctoral program in the molecular imaging laboratory, Yonsei University. His current research topics are Monte Carlo simulations for medical imaging device modeling.

Chan Woo Park received a BSc from the department of radiological science at Yonsei University, South Korea, in 2014. He is currently pursuing his master's degree in the molecular imaging laboratory at the same university. His research interests include gamma tomography systems, PET, and gamma camera systems.

Yong Hyun Chung has been a Professor in the Department of Radiation Convergence Engineering at Yonsei University since 2006. He received his BSc, MSc, and Ph.D. from the department of nuclear and quantum engineering at KAIST, South Korea, and majored in radiation detection and medical imaging, especially for nuclear medicine instrumentations. From 2002 to 2006, he worked as a Researcher in the Department of Nuclear Medicine, Samsung Medical Center, Seoul, Korea, at the Center for Clinical Research, Samsung Biomedical Research Institute, Seoul, Korea, and at the Crump Institute for Molecular Imaging, David Geffen School of Medicine, UCLA, Los Angeles, USA. His current interests lie in the area of non-invasive imaging techniques, like gamma cameras, single photon emission computed tomography (SPECT), positron emission tomography (PET) and specific nuclear material (SNM) monitoring systems.